Biophysical Journal
Article

Biophysical Society

# Cardiomyopathy Mutation Alters End-to-End Junction of Tropomyosin and Reduces Calcium Sensitivity

SaiLavanyaa Sundar,[1] Michael J. Rynkiewicz,[2] Anita Ghosh,[2] William Lehman,[2] and Jeffrey R. Moore[1,*]
[1]Department of Biological Sciences, University of Massachusetts-Lowell, Lowell, Massachusetts and [2]Department of Physiology and Biophysics, Boston University School of Medicine, Boston, Massachusetts

ABSTRACT Muscle contraction is governed by tropomyosin (Tpm) shifting azimuthally between three states on F-actin (B-, C-, and M-states) in response to calcium binding to troponin and actomyosin cross-bridge formation. The Tpm coiled coil polymerizes head to tail along the long-pitch helix of F-actin to form continuous superhelical cables that wrap around the actin filaments. The end-to-end bonds formed between the N- and C-terminus of adjacent Tpm molecules define Tpm continuity and play a critical role in the ability of Tpm to cooperatively bind to actin, thus facilitating Tpm conformational switching to cooperatively propagate along F-actin. We expect that a missense mutation in this critical overlap region associated with dilated cardiomyopathy, A277V, will alter Tpm binding and thin filament activation by altering the overlap structure. Here, we used cosedimentation assays and in vitro motility assays to determine how the mutation alters Tpm binding to actin and its ability to regulate actomyosin interactions. Analytical viscometry coupled with molecular dynamics simulations showed that the A277V mutation results in enhanced Tpm end-to-end bond strength and a reduced curvature of the Tpm overlap domain. The mutant Tpm exhibited enhanced actin-Tpm binding affinity, consistent with overlap stabilization. The observed A277V-induced decrease in cooperative activation observed with regulated thin filament motility indicates that increased overlap stabilization is not correlated with Tpm-Tpm overlap binding strength or mechanical rigidity as is often assumed. Instead, A277V-induced structural changes result in local and delocalized increases in Tpm flexibility and prominent coiled-coil twisting in pseudorepeat 4. An A277V-induced decrease in $Ca^{2+}$ sensitivity, consistent with a mutation-induced bolstering of the B-state Tpm-actin electrostatic contacts and an increased Tpm troponin T1 binding affinity, was also observed.

SIGNIFICANCE Heart muscle contraction is driven by interactions of the myosin molecular motor with actin. These interactions are governed by tropomyosin (Tpm) cooperative shifting on actin in response to calcium binding to troponin. A critical aspect of this regulation is the ability of Tpm to form a continuous cable along the actin filament via Tpm end-to-end association. In the current report, we show that a cardiomyopathy-linked single-residue substitution, A277V, located in the end-to-end overlap of Tpm causes both local and long-range perturbations of Tpm structure. Our results provide molecular-level insight into the functional alterations caused by the A277V mutation as well as specific information about the mechanism behind the hyposensitization to calcium that is often associated with dilated cardiomyopathy.

## INTRODUCTION

Dilated cardiomyopathy (DCM), characterized by the presence of left ventricular hypertrophy and impaired systolic function, is a major cause of heart failure and arrhythmia and is known to affect 1 in 250 individuals (1). A clear mechanistic cause for DCM is not known even though this idiopathic and generally familial disease is the leading cause for heart transplantation (1). Inherited DCM can be caused by mutations in sarcomeric proteins, including the well-known and thoroughly investigated thin filament gatekeeper tropomyosin (Tpm) (2,3). At least 12 missense mutations in the *TPM1* gene, encoding for the major cardiac muscle isoform of Tpm ($\alpha$-tropomyosin, also known as Tpm1.1) have been linked to the development of DCM (3). However, information about the initial stages of the disease and, in the current investigation, specific effects

*Submitted August 30, 2019, and accepted for publication November 18, 2019.*

*Correspondence: jeffrey_moore@uml.edu

Editor: David Thomas.
https://doi.org/10.1016/j.bpj.2019.11.3396

of the A277V mutation on muscle regulation are not well-documented. Thus, in this case and others, further exploration of DCM-specific phenotypes and their underlying causes is required.

The muscle thin filament is primarily composed of F-actin, Tpm, and troponin. Each 42-nm-long Tpm dimer binds alongside seven successive actin subunits, where Tpm molecules linked head to tail then form an uninterrupted cable structure that wraps around the actin thin filament (4,5). One troponin complex, made up of the subunits TnT, TnI, and TnC, binds each Tpm dimer, and the troponin-Tpm association confers $Ca^{2+}$ sensitivity to thin filament association with the myosin cross-bridge (5). The finely tuned interactions between these thin filament proteins govern muscle contraction, producing a cooperatively regulated on-off switching mechanism, with rapid activation and relaxation (6,7). As described by the McKillop and Geeves three-state model (8,9) and confirmed structurally (10–12), the cooperative regulation of cardiac and skeletal muscle depends on the azimuthal position changes of Tpm on actin under the influence of $Ca^{2+}$ and myosin binding. In the absence of $Ca^{2+}$, Tpm remains in a blocking B-state position on actin, preventing the formation of actomyosin cross-bridges. With the binding of $Ca^{2+}$ to TnC, Tpm transitions to an intermediate off-state (i.e., closed (C-state)) position on actin, partially exposing myosin binding sites on actin and allowing myosin weak binding. Actin-myosin interactions lead to further Tpm movement on actin to an open (M-state) position, enabling formation of high-affinity actomyosin cross-bridges and force production (9). The three conformational states of Tpm in the sarcomere result from a cooperative, azimuthally directed shift, which is fundamental to the on-off switching mechanism (5,13,14) that ultimately controls heart muscle contraction during each heartbeat. Previous studies on DCM-linked Tpm mutations have shown both local and delocalized structural alterations in Tpm-Tpm and in Tpm-actin interactions (15–17). However, these studies indicate that such alterations may be mutation specific and not a result of an effect common to the different mutations. Thus, one cannot ascribe a common rule to explain Tpm-based DCM mutations. The Tpm-actin affinity, in conjunction with the binding of troponin, is thus an important factor in cardiac muscle regulation, with the Tpm overlap domain both conferring structural continuity to the entire length of the Tpm cable (5,13,18) and serving as an anchor point for the associating troponin via the Tpm-binding subunit TnT (19,20). Considering the essential role played by the overlap domain in troponin contacts and conferring connectivity along the Tpm chain on F-actin, it follows that disease-linked mutations at this region of Tpm might affect Tpm cooperative activation and, hence, cardiac muscle function (21).

In this study, we determined the effect of a DCM-causing $\alpha$-Tpm mutation in the Tpm overlap domain A277V using molecular dynamics simulations. Because of its positioning at the "*d* position" in the Tpm heptad repeat structure (15,16) in the hydrophobic core of the Tpm overlap domain (Fig. 1), the mutation disrupted the tightly packed canonical overlap domain due to steric hindrances with neighboring residues at the overlap, which ultimately resulted in an overall straighter structure compared with wild-type (WT) Tpm. These structural alterations led to an increase in Tpm-Tpm end-to-end binding strength as assessed by solution viscosity.

Despite the increase in end-to-end binding affinity for A277V Tpms along F-actin, to our surprise, our in vitro motility data for thin filaments reconstituted with A277V showed a decrease, not an increase, in cooperativity and calcium sensitivity for mutant thin filaments. The decreased calcium sensitivity is consistent with mutation-induced stabilization of Tpm in the blocking B-state (or C-state) on actin. In fact, molecular dynamics simulations of A277V Tpm on actin indicate that A277V mutation promotes long-range alterations in Tpm twist and flexibility that optimize electrostatic contacts between actin and Tpm and thus appear to underlie the altered regulatory switching. Our results demonstrate that the molecular functional defects caused by the A277V Tpm mutation are both specific and delocalized and highlight that often-assumed increases in Tpm end-to-end overlap bond strength may not necessarily correlate with increases in thin filament cooperativity.

## MATERIALS AND METHODS

### Protein purification

Myosin from chicken pectoralis muscle was purified as described by Margossian and Lowey (22) and stored in 50% glycerol. Porcine cardiac actin was extracted from acetone powder according to Spudich and Watt (23) and was polymerized to F-actin by dialysis in storage buffer (4 mM BES (N,N-Bis(2-hydroxyethyl)-2-aminoethanesulfonic acid, N,N-Bis(2-hydroxyethyl)taurine), pH 7.0, 100 mM KCl, 2 mM $MgCl_2$, 1 mM $NaN_3$, 0.5 mM ATP, and 1 mM dithiothreitol (DTT)). Tissue purified troponin complex from porcine cardiac muscle was prepared according to Potter (24).

WT and A277V $\alpha$-Tpm were prepared as previously described (25). The A277V mutant Tpm1.1 clone was purchased from Genewiz (Cambridge, MA), with the desired codon mutations confirmed via sequencing. The expression and purification of the A277V Tpm from Rosetta cells was performed as described (25). The HiTrap-Q column was omitted, and three consecutive isoelectric precipitations at pH 4.5 were performed to concentrate the Tpm, which was then pelleted and resuspended in resuspension buffer (10 mM $KH_2PO_4$, 200 mM NaCl, pH 8.0). The sample was then further dialyzed into buffer containing 80 mM NaCl and 10 mM $KH_2PO_4$ (pH 7.0) and then into buffer containing 50 mM KCl, 15 mM BES, and 4 mM $MgCl_2$, pH 7.3. The protein concentrations were determined by measuring absorbance values using a Bradford assay (Bio-Rad, Hercules, CA) at 595 nm.

Human cardiac TnT1 fragment consisting of the N-terminal residues 1–156 was prepared as described by Coulton et al. (26) and was used for cosedimentation assays involving actin and Tpm.

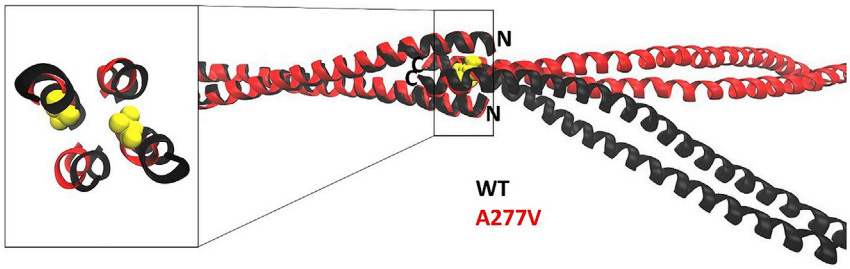


FIGURE 1 Molecular dynamics simulations of Tpm overlap domain. WT *(black ribbons)* and A277V (*red ribbons*) Tpm overlap domains are shown after superimposing the N-terminal chains of Tpm (on the *left side* of the diagram). The WT Tpm-Tpm overlap domain exhibits a curvature that matches the long pitch of F-actin helix. The Tpm A277V mutation results in an overall straighter structure and shows that subtle alteration of the overlap conformation propagates as a major decrease in coiled-coil curvature. The V277 side chain is shown in yellow van der Waals representation, showing the position of the mutation in the interface between the helices that form the overlap. The inset shows a view of the overlap looking down the superhelical axis showing the position of V277 in the four-helix bundle. The models were simulated for 30–40 ns in explicit solvent at 300 K. Parameters of the interacting coiled coils, twist angle ($\theta$), and the curvature ($\omega$) (Table 1) were compared. A277V Tpm exhibited a reduced curvature at the overlap, enabling the straightening of the Tpm molecule. Note that the WT ribbon in this view curves toward the bottom of the figure, whereas the mutant ribbon does not curve and shows a more linear conformation. To see this figure in color, go online.

## Viscosity measurements and actin cosedimentation

Viscosity measurements provide a direct assessment of Tpm end-end bond strength (21,27,28). All measurements for WT and A277V Tpm were measured in triplicate at a concentration of 1.75 mg/mL (in 10 mM imidazole, pH 7.0, 2 mM DTT, 10 mM NaCl) at room temperature (22°C) using a Cannon-Manning Semi-Micro Viscometer ($A_{50}$).

Cosedimentation of 5.0 $\mu$M F-actin in the presence of increasing concentrations of WT or A277V Tpm (0.1–3.5 $\mu$M) was performed to provide a general assessment of Tpm-actin binding affinity. Incubation of actin and Tpm in binding buffer (15 mM BES, 5 mM $MgCl_2$, 200 mM NaCl, pH 7.0) for 30 min at room temperature allowed for the actin-Tpm complex to reach binding equilibrium (29). Actin with bound Tpm was then pelleted using an Airfuge at 140,000 *g* for 30 min. The pellet (washed with the binding buffer) and supernatant bands from SDS-PAGE gels were analyzed to obtain free Tpm concentrations and the relative concentration of Tpm bound to actin, similar to Farman et al. (15).

In addition to studying the binding of Tpm to actin, cosedimentation of actin was performed to assess the binding of a TnT1 fragment to WT and A277V Tpm-actin complexes. 5.0 $\mu$M F-actin, with 3.0 $\mu$M of the specific Tpm, was allowed to incubate for 30 min at ~23°C in binding buffer (15 mM BES, 5 mM $MgCl_2$, 200 mM NaCl, pH 7.0). The actin-Tpm complexes were then cosedimented with several concentrations of TnT1 (0.1–3.5 $\mu$M) and analyzed to obtain the free TnT1 concentrations from supernatant and the relative concentration of TnT1 bound to actin-Tpm (in pellet), as described above.

## Calcium regulated in vitro motility

Regulated in vitro motility experiments were performed as described previously (30), with some modifications. Chicken skeletal muscle myosin (50 $\mu$g/mL) diluted in high-salt buffer (300 mM KCl, 25 mM BES, 5 mM EGTA, 4 mM $MgCl_2$, 10 mM DTT, pH 7.4) was added to a nitrocellulose-coated flow cell (made by forming channels between a nitrocellulose-coated coverslip and a standard glass slide with double-stick tape). Any nonspecific binding of myosin was prevented by addition of 1 mg/mL of bovine serum albumin diluted in the high-salt buffer. FITC (fluorescein isothiocyanate)-phalloidin-labeled actin filaments in low-salt buffer (55 mM KCl, 25 mM BES, 5 mM EGTA, 4 mM $MgCl_2$, 10 mM DTT, pH 7.4) were further added and allowed to interact with myosin for 1 min after two low-salt buffer washes containing 1 mM ATP and four washes with the low-salt buffer. The WT or A277V Tpm-troponin mix (600 nM) was then allowed to interact for 5 min, after which the low-salt buffer containing different $Ca^{2+}$ concentrations (pCa 4.0 to pCa 10.0) was added. FITC-labeled actin filaments (30) were observed after the addition of a scavenger mix containing 160 units of glucose oxidase and 2 $\mu$M catalase. The actin sliding velocity and percent of motile filaments under different biochemical conditions were obtained by hand-analyzing filament motility movies using an ImageJ plug-in called MTrckJ (available at https://imagescience.org/meijering/software/mtrackj/). All experiments were repeated as triplicates, and the values were averaged.

## Molecular dynamics and analysis of Tpm end-end overlap domain

Molecular dynamics simulations were performed on the overlap domain of Tpm as described by Li et al. (31). All simulations were performed in NAMD (32) in explicit solvent at 300 K and 1 atm. The model simulated for intervals of 30–40 ns consisted of residues 1–80 at the N-terminus joined to residues 205–284 at the C-terminus of an adjacent Tpm (31). After minimization, heating and equilibration steps were performed using a constant volume, with gradual release of constraints to the starting coordinates. Once the system was equilibrated at 300 K, the Langevin piston was used to maintain a constant pressure of 1 atm during production runs. Alterations in Tpm junction twist angle ($\theta$), the curvature ($\omega$), and the persistence length of the interacting coiled coils of the Tpm overlap domain structures were characterized as previously by Li et al. (31).

## Molecular dynamics of Tpm on actin

Molecular dynamics of the Tpm-F-actin complex was performed using a model that utilizes the periodic boundary conditions to create an essentially infinite filament. The initial model was derived from the cable model from previous work (4). This model was expanded to include 28 actin monomers and eight chains. This unit repeats in both directions along the filament axis by simple translation (using actin helical parameters of 27.5-Å translation and 167.1° rotation) and can therefore be modeled using a periodic boundary condition. The resulting model was solvated using the ionize, solvate, and ionize plug-ins in VMD (33) to add water, 0.15 M NaCl, and 3 mM $MgCl_2$ before molecular dynamics simulations. During the simulation, buried actin residues near the filament axis were harmonically constrained to maintain the integrity of the filament structure. Simulations were performed using NAMD. Heating to 300 K and constrained equilibrations were performed under constant volume, with gradual release of constraints on the Tpm and surface actin residues. To bring the pressure of the system to around 1 bar, a short 50,000-step run was performed under constant pressure using the Langevin piston, allowing each axis of the solvent box to change independently. The system was inspected at this point to ensure there were no gaps in the solvent or significant changes in the filament axis length. Production runs were then performed under constant volume.

This method keeps the repeat of the actin filament close to the starting value—so that the periodic boundary does not compress or elongate the filament—while bringing the pressure in the system up to a reasonable value. Simulations were continued for 40 ns.

Alterations in Tpm junction twist angle ($\theta$), the curvature ($\omega$), and the persistence length of the interacting coiled coils of the Tpm overlap domain structures were characterized as previously by Li et al. (31). Buried solvent accessible surface area (SASA) of the overlaps was calculated in VMD by adding the SASA of the N-terminal 30 residues and the C-terminal 30 residues and then subtracting the SASA of the complex (probe radius of 1.4 Å). Measurements were made on frames from the last 10 ns of simulation ($n = 500$ frames), and the values were averaged.

To calculate the electrostatic interaction energy, an average structure was calculated over the last 10 ns of simulation for the WT and A277V data using VMD, and this structure was minimized for 5000 cycles in NAMD in implicit solvent. Subsequently, the electrostatic interaction energy between the Tpm and actin chains was calculated using the NAMD Energy plug-in in VMD.

### *Statistics*

A two-tailed *t*-test in Microsoft Excel was used to determine the significant differences in viscosity of WT and A277V Tpm ($p < 0.01$). For cosedimentation assay results, data were plotted using the GraphPad Prism 8.0.2 software and fit to the "Specific Binding with Hill Slope" curve. Statistical significance was determined based on the 95% confidence of the WT and mutant Tpm data fits. For in vitro motility assay, data represent the average velocity and average percent motile of triplicate data sets. Statistical significance of $pCa_{50}$ and Hill coefficient ($n_H$) values were determined based on the 95% confidence of WT and mutant Tpm data fits for the velocity and percent motile relationships.

## RESULTS

### A277V reduces Tpm curvature and forms stronger end-end bonds

Our earlier computational work on isolated Tpm has shown that the curvature of Tpm, free of actin, closely mimics the helical pitch of F-actin. This gradual bending continues into the overlap domain and is thought to minimize the entropic cost for Tpm polymerization on actin (16,31,34). The substitution of a bulkier valine side chain at the hydrophobic core of the overlap may expand the overlap domain, thereby altering its intrinsic structural properties. Here, the A277V-containing Tpm overlap was modeled in silico, molecular dynamics was performed, and results were compared with that of WT Tpm (Fig. 1; Table 1). No significant differences in twist angle ($\theta$) were observed between the WT (93.9 ± 2.1°) and A277V (95.0 ± 2.3°) Tpms. However, a >2-fold reduction in the curvature ($\omega$) was observed for Tpm harboring the A277V mutation compared with WT Tpm (9.0 ± 3.7° vs. 3.7 ± 1.9°). The reduced curvature observed with the A277V mutation is evident in Fig. 1 as an obvious straightening of the Tpm overlap structure. In addition, the variance in curvature is also diminished during the A277V simulation, consistent with the increased persistence length of the mutant overlap construct when compared with WT.

Viscosity measurements of Tpm provide a direct measurement of Tpm end-to-end polymerization and, thus, bond strength (26–28,35,36). To determine the functional effects of the altered Tpm-Tpm binding interactions (Fig. 1), we measured isolated WT Tpm viscosity and the corresponding effect of the A277V-induced structural alterations. Under our set of conditions (Fig. 2), A277V is 2.5 times more viscous than WT, paralleling the structural alterations in the end-to-end bond seen in molecular dynamics simulations.

### The A277V mutation increases Tpm affinity for F-actin

The shape complementarity between Tpm and F-actin, along with electrostatic interactions between the two proteins, has been well-documented to facilitate thin filament assembly (16,31,37,38). These interactions are, however, relatively weak, and gap-free binding of the Tpm cable on F-actin relies on Tpm-Tpm end-to-end linkage (5,16,30). Given the effects of the A277V mutation on Tpm-Tpm structure, we therefore determined the effect of A277V on the equilibrium binding of Tpm to F-actin. The affinity of the WT and A277V Tpm to F-actin was determined by performing actin cosedimentation assays. A representative SDS-PAGE gel used to determine Tpm affinity is shown in Fig. 3. As seen in Fig. 3 *A*, the band intensity of the pelleted actin (upper band) remains relatively constant across all the lanes, whereas the Tpm band intensity (3.5–0.1 $\mu$M in the lower band) decreases from highest to lowest. The WT supernatants, on the other hand, show a very low

**TABLE 1 Analysis of the Overlap Geometry from Molecular Dynamics Simulations of the WT and A277V Tpm**

| | Isolated Overlap Domain | | On Actin in a Polymeric Cable | |
|---|---|---|---|---|
| Measurement | WT | A277V | WT | A277V |
| Curvature C- versus N-terminal fragments ($\omega$) | 8.99 ± 3.73 | 3.70 ± 1.93 | 10.10 ± 3.31 | 7.83 ± 3.40 |
| Twist angle of C- versus N-terminal fragments ($\theta$) | 93.88 ± 2.07 | 94.97 ± 2.30 | 86.53 ± 3.12 | 88.04 ± 3.08 |
| Buried SASA (Å$^2$) | 2374.03 ± 65.24 | 2410.34 ± 66.50 | 2379.60 ± 66.17 | 2377.13 ± 97.56 |
| Electrostatic interaction energy with actin (kcal/mol) | – | – | −7080.39 | −6638.57 |
| Persistence length of overlap (nm) | 567 | 2124 | 720 | 681 |

Twist angle ($\theta$), curvature ($\omega$), buried SASA, electrostatic interaction energy, and persistence length measurements of WT and A277V Tpm were calculated as outlined in (31). Standard deviations are shown for data averaged over 1000 structures for the isolated overlaps. For Tpm on actin, standard deviations for $\omega$ and $\theta$ angles are shown for data averaged over 5420 structures for WT Tpm and 5184 for A277V Tpm; average of 2168 WT and 1950 mutant structures for the surface area calculations. Significant reduction in curvature and increased persistence length of the Tpm molecule are observed with the A277V Tpm.

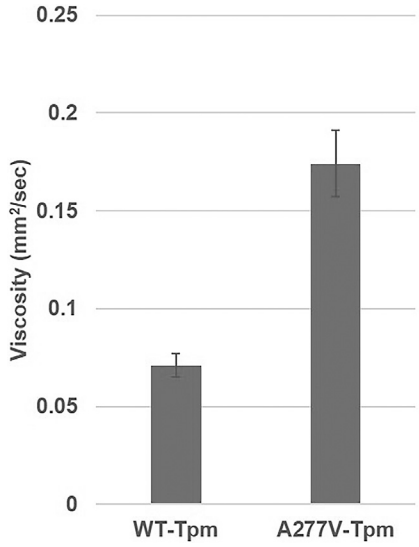


FIGURE 2 Viscosity measurements of WT and A277V Tpm. Increased viscosity of A277V Tpm represents the formation of stronger end-end bonds at the overlap domain. Data are the averages of triplicates (after subtracting viscosity of buffer) collected at 22°C with 1.75 mg/mL of Tpm (in 10 mM imidazole, pH 7.0, 2 mM DTT, 10 mM NaCl). Error bars represent standard error of the mean. Statistical significance was calculated using a two-tailed *t*-test with unequal variance ($p < 0.01$).

band intensity of actin, with decreasing concentrations of unbound Tpm. Fig. 3 *A* also shows the pellet and supernatant gels with actin and A277V Tpm. It is apparent that the A277V Tpm band intensities are higher for each corresponding concentration of Tpm tested. Gel quantification shows that the apparent affinity of the mutant Tpm to actin is ~2-fold higher than that of WT.

## A277V Tpm enhances TnT1 binding

The N- and C-terminal residues of Tpm form the four-helix bundle at the overlap domain, which interacts further with residues 82–136 of TnT (20). We therefore investigated the effect of A277V on the binding affinity of TnT1 fragment (residues 1–156, which includes the segment of TnT that binds Tpm) to actin filaments saturated with Tpm using actin cosedimentation assays. As shown in Fig. 4, the TnT1 fragment was observed to bind with a 3.5-fold-higher affinity to mutant Tpm on actin than to WT.

## A277V Tpm decreases $Ca^{2+}$ sensitivity

To test whether the mutation-induced alterations in Tpm structure and biochemistry observed alter cooperative activation of contractility by calcium, we determined the influence of the Tpm mutation on actin sliding velocity over myosin and the percent of fully $Ca^{2+}$-regulated motile filaments using the in vitro motility assay. As shown in Fig. 5, both the WT and A277V Tpms inhibited actomyosin interaction at low $Ca^{2+}$ concentrations in the presence of troponin. With increasing $Ca^{2+}$, the actin filaments activated cooperatively until saturation was reached. No significant differences were observed in the maximal sliding velocity or percent motile at saturating calcium concentrations. However, thin filaments containing A277V Tpm required higher concentrations of $Ca^{2+}$ for activation than WT Tpm (decreased $pCa_{50}$; Table 2) when measured by either assessment of motility. In addition, a significant decrease in cooperativity (Table 2) was observed for A277V measured by sliding velocity.

## The A277V mutation alters Tpm flexural variance and actin interactions

To examine the structural impact of the A277V mutation and attempt to determine the underlying altered molecular interactions between mutant Tpm and actin that result in the observed functional alterations, we performed molecular

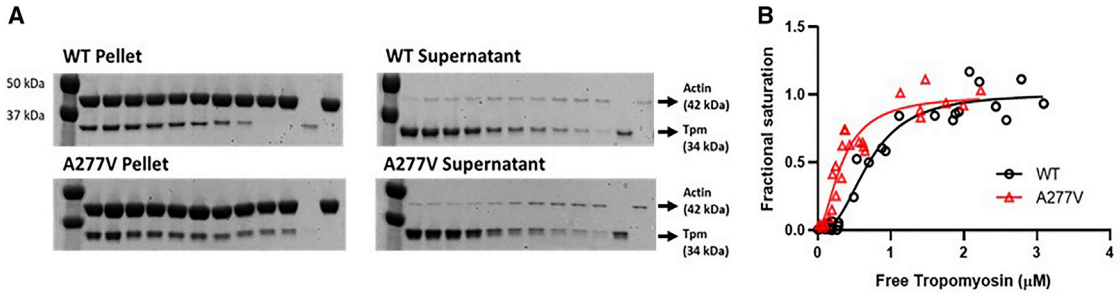


FIGURE 3 WT and mutant Tpm binding to F-actin by cosedimentation. 5.0 $\mu$M F-actin with different concentrations of Tpm (3.5–0.1 $\mu$M) were incubated for 30 min at ~23°C in binding buffer (15 mM BES, 5 mM $MgCl_2$, 200 mM NaCl, pH 7.0), followed by centrifugation using an Airfuge at 140,000 × *g* to obtain an actin pellet with bound Tpm. (*A*) Free Tpm concentrations and relative concentrations of Tpm and actin were obtained from supernatant and pellet, respectively, as band densities in 12% SDS-PAGE gels. The last two lanes on the right-hand side contain purified Tpm and actin as a control. (*B*) Data from three experimental replicates were plotted using the GraphPad Prism 8.0.2 software and fitted to the "Specific Binding with Hill Slope" fit, represented by the equation, $Y = B_{max} \times [\text{Tpm}]^h/(K_d{}^h + [\text{Tpm}]^h)$. A277V Tpm binding affinity to actin was enhanced ($K_d = 0.34 \pm 0.05$ $\mu$M, $h = 1.76 \pm 0.39$) relative to that of WT ($K_d = 0.71 \pm 0.06$ $\mu$M, $h = 2.51 \pm 0.47$). For analysis of statistical significance, see Statistics. The $K_d$ values for the WT and mutant Tpm curves are also significantly different when the data is fit to a noncooperative model with a fixed Hill coefficient of 1. To see this figure in color, go online.

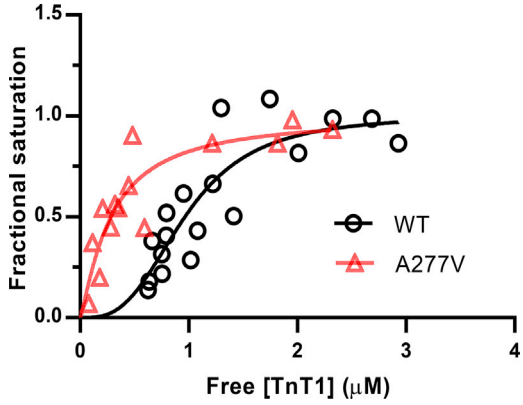


FIGURE 4 Effect of A277V Tpm on TnT1 binding to actin-Tpm by cosedimentation assay. Several concentrations (0.1–3.5 $\mu$M) of TnT1 were allowed to incubate with saturating concentrations of actin-Tpm complexes for 30 min at ~23°C in binding buffer (15 mM BES, 5 mM $MgCl_2$, 200 mM NaCl, pH 7.0). Relative concentrations of TnT1 bound to Tpm-actin and free TnT1 concentrations from triplicate data sets were plotted using the GraphPad Prism 8.0.2 software and fitted to the Hill equation, given by $Y = B_{max} \times [TnT1]^h/(K_d{}^h + [TnT1]^h)$. For analysis of statistical significance, see Statistics. To see this figure in color, go online.

dynamics simulations of WT and mutant Tpm on actin. Similar to the effects observed for the overlap domain in isolation, a reduction in the curvature ($\omega$) without a change in twist angle ($\theta$) was observed for Tpm harboring the A277V mutation compared with WT Tpm (Table 1). The mutation induces a 2.4-fold reduction in curvature of the isolated overlap domain. However, when polymeric Tpm is bound to F-actin, the curvature reduction is attenuated to 1.3-fold.

Tpm stiffness contributes to the cooperative azimuthal repositioning of Tpm regulatory movements on actin filaments. We therefore measured Tpm flexural variance during molecular dynamics as a measure of Tpm mechanical properties by quantifying mutant Tpm bending fluctuations and comparing with wild type. Local alterations in curvature and bending dynamics (local $\delta$) were observed along the length of the Tpm coiled coil (Fig. 6 *A*), which likely arise from subtle sequence variation in similar, but nonidentical, actin binding repeats (39).

As expected, the A277V mutation alters Tpm local flexibility at the N- and C-termini near the site of the mutation (Fig. 6 *A*, asterisks), likely as a result of the substitution of the conserved alanine with the larger valine side chain. This local perturbation is propagated from the site of the mutation toward the middle of the Tpm molecule, where prominent delocalized effects are observed surrounding Tpm residue 150 (Fig. 6 *A*, arrows).

Our earlier work showed that, in addition to the flexural variance described above, subtle cumulative twisting of the Tpm coiled coil is critical to assure strong alignment between Tpm-actin electrostatic contacts (17,39). Fig. 6 *B* shows that the introduction of the A277V mutation causes a prominent overtwist surrounding Tpm 150 (~130–160), which underlies the increased flexibility observed in this region and likely represents a compensatory structural modification to accommodate the straightening of the A277V Tpm overlap domain in the polymeric cable.

The A277V-induced overtwist is located near Tpm E139, a charged residue thought to be critical for binding a cluster of positively charged amino acid side chains on actin (17,40). The overtwist, which can be clearly seen in Fig. 7, places negatively charged Tpm residues E138, E142, and E145 closer to and in a better position to interact with the positive cluster on actin of R147, K326, and K328 (Fig. 7; Table 3). These interactions likely contribute to increased Tpm-actin electrostatic interaction energy (Table 1) and B-state stabilization observed for A277V Tpm.

## DISCUSSION

In this study, we used molecular dynamics simulations, solution biochemistry, and in vitro motility assays to examine the direct molecular effects of the A277V mutation of Tpm on its structure and function. Viscosity measurements indicate that A277V-induced structural alterations result in a stronger junctional bond between the N- and C-terminal domains between adjacent Tpm molecules. This effect can be ascribed directly to substitution of alanine by valine and its bulkier side chain. In turn, the substitution caused an overall straightening and apparent stiffening of

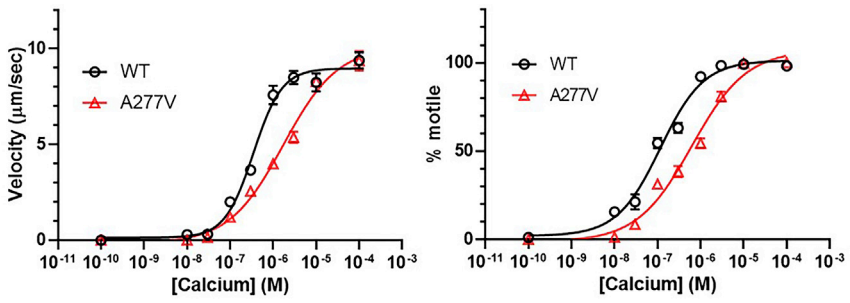


FIGURE 5 Effect of WT and mutant Tpm on actin sliding velocity and percent motile were evaluated using in vitro motility assay. (*A*) Velocity change with increasing [$Ca^{2+}$] showed a decreased $pCa_{50}$, representing a decrease in calcium sensitivity for thin filaments with the A277V Tpm. A similar result was observed with the data in (*B*) percent motile versus [$Ca^{2+}$], representative of a decrease in calcium sensitivity (decrease in $pCa_{50}$) with the A277V Tpm. Each data point is the average of triplicates, and the error bars represent the mean ± SE. The data in both (*A*) and (*B*) were plotted using the GraphPad Prism 8.0.2 software and fitted to the Hill equation, given by $Y = \text{Offset} + ([Ca^{2+}]^n{}_H) \times (V_{max} - \text{Offset})/([Ca^{2+}]^n{}_H + pCa_{50}{}^n{}_H)$, where $n_H$ is the Hill coefficient. For analysis of statistical significance, see Statistics. To see this figure in color, go online.

**TABLE 2 $pCa_{50}$ and Hill Coefficient ($n_H$) Values Calculated for WT and Mutant Tpm, from Velocity and Percent Motile Data**

| Tpm | Velocity $pCa_{50}$ | Velocity Hill Coefficient $n_H$ | Percent Motile $pCa_{50}$ | Percent Motility Hill Coefficient $n_H$ |
|---|---|---|---|---|
| WT | 6.46 ± 0.19 | 1.31 ± 0.25 | 6.94 ± 0.29 | 0.86 ± 0.16 |
| A277V | 5.76 ± 0.34[a] | 0.69 ± 0.12 | 6.20 ± 0.43[a] | 0.68 ± 0.15 |

Data are velocity and percent motile data from Fig. 4. Data are averages of triplicates; mean ± SE included as error values.[a]Statistical significance of differences determined by 95% confidence interval of data fit compared with WT Tpm data fit.

the Tpm-Tpm end-to-end complex. In order for A277V to then bind properly to F-actin, the conformational anomaly must be compensated elsewhere along the Tpm dimer, reminiscent of the extra stiffening caused by the Tpm mutation D137L, resulting in delocalized flexibility distant from the mutation (16,39,41). Similar to long-range effects seen with the D137L Tpm mutation, we also observe a delocalized response: here, a hypertwisting of the centrally located Tpm domains distant from the mutation site.

Using regulated in vitro motility assays, we showed that the A277V mutation decreased calcium sensitivity and cooperativity of activation (Fig. 5) despite the increased Tpm-Tpm binding strength. The decreased calcium sensitivity can be readily explained by the hypertwisting of the mutant Tpm stabilizing actin-Tpm B-state interactions, and the decreased cooperativity is consistent with the increased flexibility of the mutant Tpm molecule adjacent to the hypertwisted region. Furthermore, we show that mutation-induced increases in TnT-Tpm affinity may additionally underlie alterations in calcium regulation by the thin filament.

Tpm is a parallel $\alpha$-helical coiled-coil dimer that consists of multiple short-range repeating heptad motifs, *a, b, c, d, e, f,* and *g,* where the *a* and *d* positions are typically hydrophobic residues that stabilize the Tpm dimer by packing as canonical knobs-into-holes configuration (42,43). For higher-order oligomers of coiled-coil proteins, such as the four-helix bundle found in the Tpm overlap, the *a* and *d* residues of the heptads can form knobs into holes, packing with adjacent helices (44). The A277V mutation resides in the *d* position of the heptad repeat structure and thus interacts with nearby hydrophobic residues forming the core of the Tpm bundle (Fig. 1). Another longer-range repeating pattern in Tpm consists of clusters of alanine (or serine) residues that are interspersed at the *a* and *d* positions. Alanines introduce a slight axial shift between the Tpm molecules in the dimer and thus are responsible for the curved native structure of Tpm (45). Like the *a* and *d* residues in the Ala clusters of the Tpm coiled coil, A277 is in a similar position in the four-helix bundle, allowing the component helices surrounding the hydrophobic core to move closer to each other. Consistent with this role for alanine, our in silico studies on the Tpm overlap domain revealed that substitution of the alanine at positon 277 with valine resulted in a reduction in curvature, with no significant alterations in twist, resulting in an overall straightening of the Tpm molecule (Fig. 1; Table 1).

This straightening of the molecule (Fig. 1) and increased end-to-end bond formation (Fig. 2) indicate that the valine substitution ultimately results in a stronger hydrophobic core at the four-helix bundle. Recently published thermal denaturation studies on the A277V Tpm by Matyushenko et al. (21) also suggest the stabilization of the C-terminus of Tpm, consistent with the formation of stronger end-to-end bonds. However, they did not find differences between the WT and A277V Tpm viscosity, which may be attributable to their use of higher ionic strength and lower protein concentration, as was done here to maximize end-to-end binding; in addition, their application of falling ball viscometry may have been less sensitive than is possible by implementing Cannon-Manning Semi-Micro viscometers.

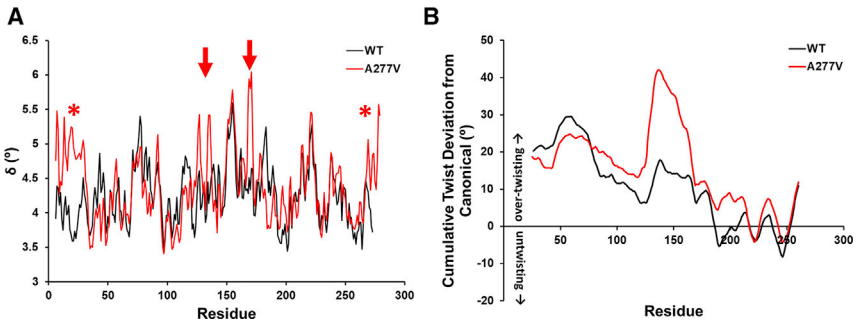


FIGURE 6 Local angular deviations from the average structure and cumulative twisting variance during molecular dynamics. (*A*) Shown is a comparison of A277V mutation-induced local changes in flexibility ($\delta$) of Tpm on F-actin. WT is shown in black, and A277V is shown in red. Asterisks and arrows indicate regions of increased flexibility in A277V Tpm, in both the overlap as well as the center of the Tpm molecule. Values of $\delta$ were calculated as previously described (34). The local deltas were calculated by averaging the measured $\delta$ angles centered over each residue for 1425 molecular dynamics structures for the mutant and 1000 structures for the WT. (*B*) Shown is the comparison of local twisting of WT (*black*) and A277V (*red*) Tpm on F-actin during molecular dynamics simulations, calculated as previously described (39). The twisting was averaged over each residue for 200 molecular dynamics trajectories for the mutant and 3000 for the WT. Local overtwisting or untwisting compared with a canonical coiled-coil Tpm is indicated. Note that there is a pronounced overtwisting effect in the middle of the A277V molecule as a consequence of the mutation in the overlap domain. To see this figure in color, go online.

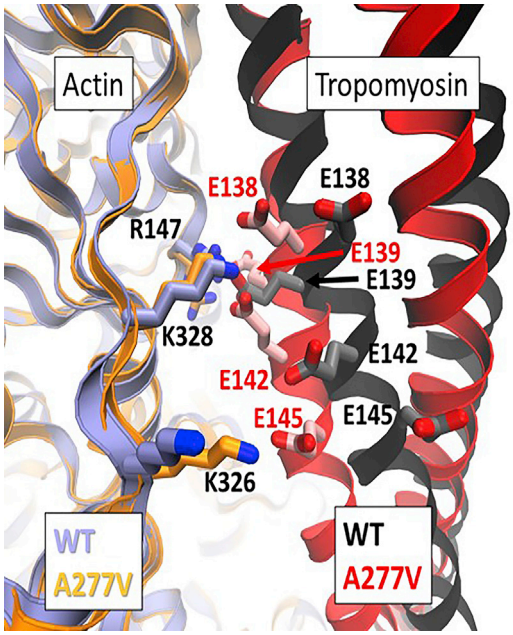


FIGURE 7 Distinctions in molecular structure of WT and mutant Tpm. Shown is a superposition of the minimized, average structures from the simulations of WT Tpm (*black ribbons*) and A277V Tpm (*red ribbons*) on the continuous actin filament (*purple* and *yellow ribbons*). Note differences in backbone and side-chain conformation between WT and A277V Tpm. Selected residues of actin (on the *left*) and Tpm (helices on the *right*) are highlighted in stick for the WT (*gray carbons*) and A277V (*pink carbons*). Note that the region displayed here reflects the region showing the marked deviation in the twisting of Tpm in Fig. 6 *B*. This twisting positions Tpm residues E139, E142, and E145 in the mutant Tpm much closer to the positively charged actin residues R147, K326, and K328, thus forming novel, close salt bridge interactions not present in the WT model. These interactions contribute to the greater electrostatic interaction energy measured between actin and A277V Tpm when compared with WT, suggesting a mechanism for the observed changes in calcium sensitivity observed in the motility assays. To see this figure in color, go online.

Our in vitro motility assays showed significant reduction in cooperativity and calcium sensitivity, which is consistent with altered actin contacts. The hyposensitization to calcium and decreased cooperativity observed here agree with a number of previously studied DCM-associated mutations (15,46,47). Still, it might appear to be counterintuitive that the formation of stronger end-to-end bonds and a straightening of the whole Tpm molecule are at the root of a decrease in cooperative activation of thin filaments. Our MD simulations show that alteration at the overlap domain of Tpm propagates structural alterations along the whole Tpm cable on actin, leading to alterations in specific actin-Tpm contacts. Our data from cosedimentation assays, depicting a higher affinity of Tpm binding to F-actin, are consistent with increased Tpm-Tpm end-to-end bond strength but might also result from the observed molecular alterations in Tpm-actin contacts, facilitating the positioning of Tpm in the B-state on actin and thus contributing to the observed decreased calcium sensitivity.

**TABLE 3 Close Electrostatic Contacts between Tpm Pseudorepeat-4 and F-Actin**

| Actin Residue | Tpm Residue | Wild Type | A277V |
|---|---|---|---|
| Lys 128 | Glu 138 | 6.24 Å | 2.66 Å |
| Arg 147 | Glu 129 | 2.64 Å | 2.72 Å |
| Lys 328 | Glu 139 | 2.71 Å | 7.07 Å |
| Lys 328 | Glu 142 | 6.33 Å | 2.69 Å |
| Lys 326 | Glu 145 | 12.16 Å | 2.72 Å |

Salt bridge distances in minimized, average structures from molecular dynamics simulations. Distances are measured in VMD from the closest non-hydrogen side-chain atoms. Note the closer contacts in the mutant Tpm compared with the wild type.

In the muscle thin filament, TnT binds to Tpm in an antiparallel manner, with the N-terminus of TnT extending over the overlap domain. Our data show that the A277V mutation increases the affinity of the TnT N-terminus for actin-Tpm. The C-terminal 20 amino acids of striated muscle Tpm (263–284) have been shown to have a number of residues with large side chains in the hydrophobic core that destabilize the dimeric coiled-coiled conformation by causing the Tpm $\alpha$-helices to splay apart. In this splayed conformation, the *a* and *d* side chains of one Tpm in the dimer form the classic knobs-into-holes patterning, whereas their counterparts on the other Tpm molecule are oriented away from the core and have been proposed to play a role in TnT1 binding (42). The substitution of the alanine at position 277 in Tpm with a bulky valine would further favor splaying, which is consistent with the increased TnT1 affinity observed here for the mutant Tpm on actin.

Previous reports show that suppression of cTnT causes a reduction in contractility in vivo (48). Furthermore, DCM-causing TnT1 mutations, located close to the Tpm overlap in cardiac thin filaments, also result in a hyposensitization to calcium due to altered TnT-Tpm binding affinity (48). A stabilization of the Tpm in the B-state (or C-state) via a stronger binding of TnT to semiflexible Tpm would result in decreased calcium sensitivity and decreased cooperativity, as observed here, suggesting that in addition to the observed Tpm structural and mechanical changes observed, alterations in TnT-Tpm interactions can be a critical determinant in cardiomyopathy mutations. This approach involving in situ and in vitro techniques helps offer a multifaceted strategy to understanding the effect of mutation-linked diseases at a molecular level, providing specific information to promote exploratory studies on potential therapeutic drug targets.

## AUTHOR CONTRIBUTIONS

S.S. performed research, analyzed data, and wrote the manuscript. M.J.R. carried out molecular dynamics simulations and analyzed data. A.G. prepared the TnT1 protein fragment. W.L. designed research and wrote the manuscript. J.R.M. designed research and wrote the manuscript.

## ACKNOWLEDGMENTS

The authors thank Dr. Alice W. Racca for insightful discussions.

These studies were supported by National Institutes of Health grants R01HL036153 (to W.L.), R01HL123774 (to J.R.M. and W.L.), and American Heart Association 20PRE35120307 (to S.S.). The Massachusetts Green High Performance Computing Center provided considerable computational resources.

## REFERENCES

1. Wilcox, J. E., and R. E. Hershberger. 2018. Genetic cardiomyopathies. *Curr. Opin. Cardiol.* 33:354–362.
2. Lakdawala, N. K., L. Dellefave, …, C. Y. Ho. 2010. Familial dilated cardiomyopathy caused by an alpha-tropomyosin mutation: the distinctive natural history of sarcomeric dilated cardiomyopathy. *J. Am. Coll. Cardiol.* 55:320–329.
3. Redwood, C., and P. Robinson. 2013. Alpha-tropomyosin mutations in inherited cardiomyopathies. *J. Muscle Res. Cell Motil.* 34:285–294.
4. Orzechowski, M., X. E. Li, …, W. Lehman. 2014. An atomic model of the tropomyosin cable on F-actin. *Biophys. J.* 107:694–699.
5. Moore, J. R., S. G. Campbell, and W. Lehman. 2016. Structural determinants of muscle thin filament cooperativity. *Arch. Biochem. Biophys.* 594:8–17.
6. Tobacman, L. S. 1996. Thin filament-mediated regulation of cardiac contraction. *Annu. Rev. Physiol.* 58:447–481.
7. Galińska-Rakoczy, A., P. Engel, …, W. Lehman. 2008. Structural basis for the regulation of muscle contraction by troponin and tropomyosin. *J. Mol. Biol.* 379:929–935.
8. McKillop, D. F., and M. A. Geeves. 1993. Regulation of the interaction between actin and myosin subfragment 1: evidence for three states of the thin filament. *Biophys. J.* 65:693–701.
9. Lehman, W. 2017. Switching muscles on and off in steps: the McKillop-Geeves three-state model of muscle regulation. *Biophys. J.* 112:2459–2466.
10. Holmes, K. C. 1995. The actomyosin interaction and its control by tropomyosin. *Biophys. J.* 68 (*Suppl*):2S–5S, discussion 6S–7S.
11. Lehman, W., R. Craig, and P. Vibert. 1994. Ca(2+)-induced tropomyosin movement in Limulus thin filaments revealed by three-dimensional reconstruction. *Nature.* 368:65–67.
12. Vibert, P., R. Craig, and W. Lehman. 1997. Steric-model for activation of muscle thin filaments. *J. Mol. Biol.* 266:8–14.
13. Li, X. E., M. Orzechowski, …, S. Fischer. 2014. Structure and flexibility of the tropomyosin overlap junction. *Biochem. Biophys. Res. Commun.* 446:304–308.
14. Lehman, W., X. E. Li, …, S. Fischer. 2014. The structural dynamics of α-tropomyosin on F-actin shape the overlap complex between adjacent tropomyosin molecules. *Arch. Biochem. Biophys.* 552-553:68–73.
15. Farman, G. P., M. J. Rynkiewicz, …, J. R. Moore. 2018. HCM and DCM cardiomyopathy-linked α-tropomyosin mutations influence off-state stability and crossbridge interaction on thin filaments. *Arch. Biochem. Biophys.* 647:84–92.
16. Lehman, W., M. J. Rynkiewicz, and J. R. Moore. 2019. A new twist on tropomyosin binding to actin filaments: perspectives on thin filament function, assembly and biomechanics. *J. Muscle Res. Cell Motil*.
17. Lehman, W., J. R. Moore, …, M. J. Rynkiewicz. 2019. The effect of tropomyosin mutations on actin-tropomyosin binding: in search of lost time. *Biophys. J.* 116:2275–2284.
18. Greenfield, N. J., Y. J. Huang, …, S. E. Hitchcock-DeGregori. 2006. Solution NMR structure of the junction between tropomyosin molecules: implications for actin binding and regulation. *J. Mol. Biol.* 364:80–96.
19. Marston, S., and J. E. Zamora. 2019. Troponin structure and function: a view of recent progress. *J. Muscle Res. Cell Motil*.
20. Palm, T., N. J. Greenfield, and S. E. Hitchcock-DeGregori. 2003. Tropomyosin ends determine the stability and functionality of overlap and troponin T complexes. *Biophys. J.* 84:3181–3189.
21. Matyushenko, A. M., N. A. Koubassova, …, A. K. Tsaturyan. 2019. The effects of cardiomyopathy-associated mutations in the head-to-tail overlap junction of α-tropomyosin on its properties and interaction with actin. *Int. J. Biol. Macromol.* 125:1266–1274.
22. Margossian, S. S., and S. Lowey. 1982. Preparation of myosin and its subfragments from rabbit skeletal muscle. *Methods Enzymol.* 85:55–71.
23. Spudich, J. A., and S. Watt. 1971. The regulation of rabbit skeletal muscle contraction. I. Biochemical studies of the interaction of the tropomyosin-troponin complex with actin and the proteolytic fragments of myosin. *J. Biol. Chem.* 246:4866–4871.
24. Potter, J. D. 1982. Preparation of troponin and its subunits. *Methods Enzymol.* 85:241–263.
25. Orzechowski, M., S. Fischer, …, G. P. Farman. 2014. Energy landscapes reveal the myopathic effects of tropomyosin mutations. *Arch. Biochem. Biophys.* 564:89–99.
26. Coulton, A. T., K. Koka, …, M. A. Geeves. 2008. Role of the head-to-tail overlap region in smooth and skeletal muscle beta-tropomyosin. *Biochemistry.* 47:388–397.
27. Sousa, A. D., and C. S. Farah. 2002. Quantitative analysis of tropomyosin linear polymerization equilibrium as a function of ionic strength. *J. Biol. Chem.* 277:2081–2088.
28. Hilario, E., S. L. da Silva, …, M. C. Bertolini. 2004. Effects of cardiomyopathic mutations on the biochemical and biophysical properties of the human alpha-tropomyosin. *Eur. J. Biochem.* 271:4132–4140.
29. Heier, J. A., D. J. Dickinson, and A. V. Kwiatkowski. 2017. Measuring protein binding to F-actin by co-sedimentation. *J. Vis. Exp* 55613.
30. Rynkiewicz, M. J., T. Prum, …, W. Lehman. 2017. Tropomyosin must interact weakly with actin to effectively regulate thin filament function. *Biophys. J.* 113:2444–2451.
31. Li, X. E., K. C. Holmes, …, S. Fischer. 2010. The shape and flexibility of tropomyosin coiled coils: implications for actin filament assembly and regulation. *J. Mol. Biol.* 395:327–339.
32. Phillips, J. C., R. Braun, …, K. Schulten. 2005. Scalable molecular dynamics with NAMD. *J. Comput. Chem.* 26:1781–1802.
33. Humphrey, W., A. Dalke, and K. Schulten. 1996. VMD: visual molecular dynamics. *J. Mol. Graph.* 14:33–38, 27–28..
34. Li, X. E., W. Lehman, …, K. C. Holmes. 2010. Curvature variation along the tropomyosin molecule. *J. Struct. Biol.* 170:307–312.
35. Drabikowski, W., and E. Nowak. 1968. Studies on the interaction of F-actin with tropomyosin. *Eur. J. Biochem.* 5:376–384.
36. Ooi, T., K. Mihashi, and H. Kobayashi. 1962. On the polymerization of tropomyosin. *Arch. Biochem. Biophys.* 98:1–11.
37. Zheng, W., B. Barua, and S. E. Hitchcock-DeGregori. 2013. Probing the flexibility of tropomyosin and its binding to filamentous actin using molecular dynamics simulations. *Biophys. J.* 105:1882–1892.
38. Barua, B., M. C. Pamula, and S. E. Hitchcock-DeGregori. 2011. Evolutionarily conserved surface residues constitute actin binding sites of tropomyosin. *Proc. Natl. Acad. Sci. USA.* 108:10150–10155.
39. Lehman, W., X. Li, …, M. J. Rynkiewicz. 2018. Precise binding of tropomyosin on actin involves sequence-dependent variance in coiled-coil twisting. *Biophys. J.* 115:1082–1092.
40. Dominguez, R. 2011. Tropomyosin: the gatekeeper's view of the actin filament revealed. *Biophys. J.* 100:797–798.
41. Moore, J. R., X. Li, …, W. Lehman. 2011. Structural implications of conserved aspartate residues located in tropomyosin's coiled-coil core. *Bioarchitecture.* 1:250–255.
42. Li, Y., S. Mui, …, C. Cohen. 2002. The crystal structure of the C-terminal fragment of striated-muscle alpha-tropomyosin reveals a key troponin T recognition site. *Proc. Natl. Acad. Sci. USA.* 99:7378–7383.
43. Crick, F. H. C., and I. U. Cr. 1953. The packing of α-helices: simple coiled-coils. *Acta Crystallogr.* 6:689–697.

44. Lupas, A. 1996. Coiled coils: new structures and new functions. *Trends Biochem. Sci.* 21:375–382.

45. Brown, J. H., K. H. Kim, …, C. Cohen. 2001. Deciphering the design of the tropomyosin molecule. *Proc. Natl. Acad. Sci. USA.* 98:8496–8501.

46. Ly, T., C. T. Pappas, …, A. S. Kostyukova. 2019. Effects of cardiomyopathy-linked mutations K15N and R21H in tropomyosin on thin-filament regulation and pointed-end dynamics. *Mol. Biol. Cell.* 30:268–281.

47. Lynn, M. L., L. Tal Grinspan, …, J. C. Tardiff. 2017. The structural basis of alpha-tropomyosin linked (Asp230Asn) familial dilated cardiomyopathy. *J. Mol. Cell. Cardiol.* 108:127–137.

48. Toyota, N., H. Takano-Ohmuro, …, F. Suzuki-Toyota. 2008. Suppression of cardiac troponin T induces reduction of contractility and structural disorganization in chicken cardiomyocytes. *Cell Struct. Funct.* 33:193–201.